Award Number:
W81XWH-13-1-0415

TITLE:

Testing Brain Overgrowth and Synaptic Models of Autism Using NPC's and Neurons from Patient-Derived IPS Cells

PRINCIPAL INVESTIGATOR:
Anthony Wynshaw-Boris, MD, PhD

CONTRACTING ORGANIZATION:

Case Western Reserve University
Cleveland, OH 44106-4955

REPORT DATE: December 2015

TYPE OF REPORT: FINAL

PREPARED FOR: U.S. Army Medical Research and Materiel Command
Fort Detrick, Maryland 21702-5012

DISTRIBUTION STATEMENT:

X Approved for public release; distribution unlimited

REPORT DOCUMENTATION PAGE

Form Approved
OMB No. 0704-0188

1. REPORT DATE	2. REPORT TYPE	3. DATES COVERED
December 2015	Final	15 Sept 2013 – 14 Sept 2015

4. TITLE AND SUBTITLE
Testing Brain Overgrowth and Synaptic Models of Autism Using NPC's and Neurons from Patient-Derived IPS Cells

5a. CONTRACT NUMBER

5b. GRANT NUMBER
W81XWH-13-1-0415

5c. PROGRAM ELEMENT NUMBER

6. AUTHOR(S)
Anthony Wynshaw-Boris, MD, PhD

E-Mail: ajw168@case.edu

5d. PROJECT NUMBER

5e. TASK NUMBER

5f. WORK UNIT NUMBER

7. PERFORMING ORGANIZATION NAME(S) AND ADDRESS(ES)

Case Western Reserve University
Cleveland, OH 44106-4955

8. PERFORMING ORGANIZATION REPORT NUMBER

9. SPONSORING / MONITORING AGENCY NAME(S) AND ADDRESS(ES)

U.S. Army Medical Research and Materiel Command
Fort Detrick, Maryland 21702-5012

10. SPONSOR/MONITOR'S ACRONYM(S)

11. SPONSOR/MONITOR'S REPORT NUMBER(S)

12. DISTRIBUTION / AVAILABILITY STATEMENT

Approved for Public Release; Distribution Unlimited

13. SUPPLEMENTARY NOTES

14. ABSTRACT
Autism and autism spectrum disorders (ASD) are complex neurodevelopmental diseases that affect about 1% of children in the United States. Such disorders are characterized by deficits in verbal communication, impaired social interaction, and limited and repetitive interests and behavior. Recent studies have led to two major hypotheses for autism pathogenesis: early brain overgrowth and synaptogenesis defects. The goal of this project is to produce human cellular models of non-syndromic ASD. We used cellular reprogramming to develop iPSCs from ASD patients (and non-autistic controls) for the production of patient-derived neural progenitors (NPCs) and neurons to study cellular phenotypes that directly test whether brain overgrowth and/or synaptogenesis mechanisms are found in ASD NPCs and neurons. Patient-derived NPCs and neurons from these ASD and control individuals will be used for the functional characterization of iPSCs-derived NPCs and neurons from ASD and control individuals for potential autism-specific defects in proliferation, neural development and synaptogenesis, and for gene expression studies.

15. SUBJECT TERMS
Autism, induced pluripotent stem cells, gene expression.

16. SECURITY CLASSIFICATION OF:			17. LIMITATION OF ABSTRACT	18. NUMBER OF PAGES	19a. NAME OF RESPONSIBLE PERSON
a. REPORT	b. ABSTRACT	c. THIS PAGE			USAMRMC
Unclassified	Unclassified	Unclassified	Unclassified	18	19b. TELEPHONE NUMBER *(include area code)*

Table of Contents

1. INTRODUCTION:

Autism and autism spectrum disorders (ASD) are complex neurodevelopmental diseases that affect about 1% of children in the United States. Such disorders are characterized by deficits in verbal communication, impaired social interaction, as well as limited and repetitive interests and behavior. Recent studies have led to two major hypotheses for autism pathogenesis. First, early brain overgrowth appears to be a critical feature in the development of ASD. This hypothesis is based on MRI studies of autistic individuals (Courchesne et al. 2001; Schumann et al. 2010). A second model for the development of autism is synaptic dysregulation. This hypothesis is based on several lines of evidence, including the finding that mutations in genes coding for proteins that play important roles in synaptogenesis and synaptic function, such as MeCP2, Shank3, and the gene families for neurexin and neuroligin, are found in individuals with syndromic ASD. These pathogenic mechanisms are not mutually exclusive and may both be important for the development of ASD. The major impediment to testing these and other hypotheses about autism is the lack of relevant animal and cell models. The direct study of live brain tissue from ASD patients is impossible, and no suitable animal models can adequately reproduce the complicated structure and function of the human brain. Recently, reprogramming of human somatic cells to a pluripotent state by over-expression of specific genes into induced pluripotent stem cells, or iPSCs (Takahashi et al., 2007), has provided an exciting opportunity to produce a relevant human cellular model of complex human neurogenetic diseases (Marchetto et al. 2011). Now, iPSCs have been generated for several neurological disorders and diseases, including Rett syndrome, a syndromic ASD (Marchetto et al. 2010). The objective of this project is to produce human cellular models of ASD. Here we used cellular reprogramming to develop iPSCs from non-syndromic ASD patients (and non-autistic controls) for the production of patient-derived neural progenitors (NPCs) and neurons to study cellular phenotypes and test whether brain overgrowth and/or synaptogenesis deficits are found in ASD NPCs and neurons.

2. KEYWORDS:

Autism spectrum disorder, ASD, neurodevelopmental disease, disease modeling, induced pluripotent stem cell, iPS, human neurons, disease-in-a-dish, brain overgrowth.

3. OVERALL PROJECT SUMMARY

In our final progress report we will present combined progress from the first and the second year of the research grant. During the first year of the research grant we focused on the functional characterization of the iPSC-derived neuroprogenitors (NPCs) and neurons from ASD patients and age/gender matched neurotypical individuals. We have screened individuals for potential autism-specific defects in proliferation, neural development and synaptogenesis as proposed in the Statement of Work (SOW), Task 1. During the second year of the research grant we focused on molecular and functional characterization of the iPSC-derived neurons from ASD patients and age/gender matched neurotypical individuals. We have screened individuals for potential autism-specific differences in expression profile and defects in neuronal networks as proposed in the Statement of Work (SOW), Task 2.

Task 1: Functional characterization of iPSCs-derived NPCs and neurons from ASD and control individuals for potential autism-specific defects in proliferation, neural development and synaptogenesis (months 1-16).

1a. *Characterize ASD-iPSCs from 7 ASD patients and 6 controls (at least 2 clones for each individual) for pluripotency and neural differentiation potential (months 1-6).*

We recruited 8 ASD patients with quantitative MRI-validated early brain enlargement ranging from mild to macrencephaly and 5 age/gender-matched control individuals for skin biopsies and phenotypic characterization based on the stability of the karyotype. The ASD donors displayed larger brain size compared to the normal average brain size of typically developing control subjects at any given age (**Figure 1a, b Image courtesy from Eric Courchesne, University of California Autism Center of Excellence, La Jolla, CA**). Copy Number Variation analysis using DNA extracted from the donors' whole blood did not show the presence of any rare structural variant known to be associated with ASD unknown etiology (data not shown). ASD and non-affected control fibroblasts were transduced with 4 retroviral reprogramming vectors (Sox2, Oct4, c-Myc and Klf4), as described elsewhere Takahashi, et al. [1]. Following 2 to 3 weeks of culture in human embryonic stem cells (hESC)-supporting conditions, compact refractile ESC-like colonies emerged from a background of fibroblasts. IPSC colonies were then manually picked and cultured under feeder-free conditions. Cells were mechanically expanded for at least 10 passages and tested for the expression of pluripotent markers. We obtained several clones that continuously expressed pluripotent markers, such as Nanog, Lin28, Tra-1-81 and Sox2 from each control wild-type (WT)-iPSCs and ASD-iPSCs. We excluded all karyotypically unstable clones from further experiments (**Figure 2**).

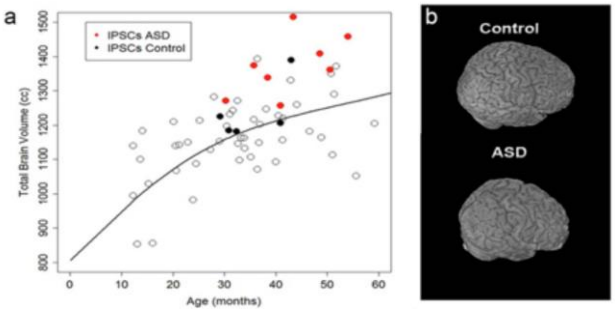

Figure 1. Derivation of NPCs from ASD and control subjects. (**a**) Left panel, scatterplot of Total Brain Volume (TBV) across ages. Open black circles indicate brain size of typically developing subjects. Black solid dots represent control donors. Red solid dots represent ASD donors. (**b**) Three-dimensional reconstructions of the brain from one control donor and one ASD donor.

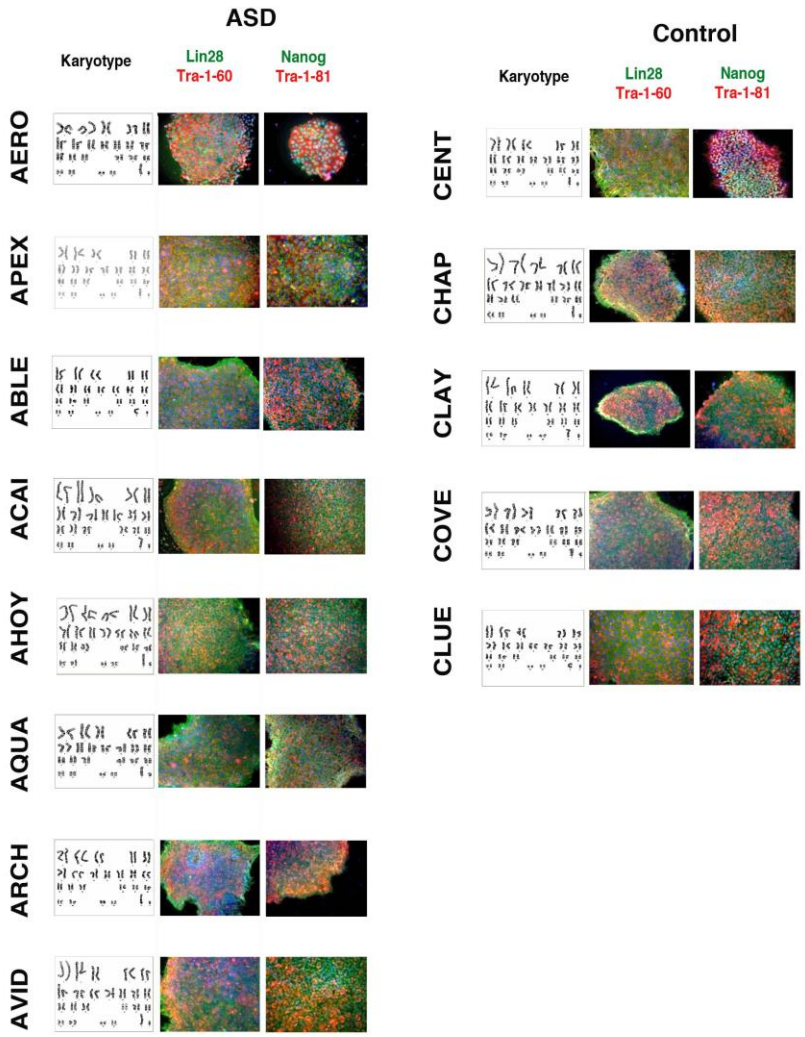

Figure 2. Characterization of iPSCs derived from controls and ASD subjects. Quality control of fibroblast reprogramming showing normal karyotype and expression of pluripotent markers for at least 2 clones of each iPSC. Scale bar: 20 µm.

The data described in **Task 1a** was generated and analyzed in Dr. Gage laboratory, Salk Institute, La Jolla, CA.

1b. *Perform NPC differentiation using the iPSCs clones characterized in 1a and access cell proliferation using the methods described below (months 6-12).*

We used our previous published protocol to generate NPCs from iPSCs [2] in the presence of Noggin. Briefly, we initiated neural differentiation by plating 1-week-old embryoid bodies (EBs) treated with Noggin. After a week in culture, EB-derived rosettes became apparent in the dish. Rosettes were then manually collected, dissociated and re-plated. The NPCs derived from rosettes formed a homogeneous population after a few passages from patients and controls, and continued to proliferate in the presence of FGF2 as adherent monolayers. We hypothesized that an alteration of the rates of NPC proliferation could result in early brain overgrowth. Proliferation was measured by calculating the population doubling time from plating at passages 3 to 7 (P3-7) in continuous culture. From P4, the population doubling time decreased in ASD NPCs from all 8 patients compared to NPCs from all 5 controls, reaching statistical significance at P6 (**Figure 3a**). Cell cycle analysis at P6 revealed that shortening of G1 and S phases was the main reason for the decrease in the population doubling time; with no change of G2-M phase length (**Figure 3b**). Double labeling for Ki67 and pHH3 revealed an increased percentage of $Ki67^{+}$ (cycling cells) in ASD relative to control NPCs, whereas the percentage of

pHH3^{+}Ki67^{+} (G2-M phase mitotic cells) was unaffected in autistic NPCs (**Figure 3c, d**). These findings demonstrate that iPSC-derived NPCs from ASD patients with macrencephaly proliferated faster than those derived from controls. Next, we characterized the expression of forebrain and midbrain markers in the ASD-derived NPCs and those from control individuals. SOX1 (a marker for maintenance of radial glial NPCs identity), and Vimentin (the intermediate filament protein of NPCs) were up-regulated in the ASD NPCs compared to control NPCs (**Figure 3e-i)**. SOX1 and Vimentin were previously shown to correlate with induced proliferation of NPCs [3,4], consistent with the increased rate of proliferation of NPCs derived from the ASD individuals. The expression of PAX6 (a marker of forebrain neural-ectoderm) and OTX2 (a marker of the midbrain and forebrain), measured by immunocytochemistry, Western blot and qPCR, were unchanged in ASD and control NPCs (**Figure 3g-i**). In addition, the expression of the intermediate NPCs marker TBR2 was low and did not differ between ASD and control NPCs (data not shown). We then investigated further the mechanism generating increased progenitor proliferation in ASD cohort. Based on previous unpublished observations we hypothesized that the aberrant proliferation in ASD-derived NPCs could be mediated by a deregulation of the □-catenin/Brn2/Tbr2 transcriptional cascade. To test our hypothesis, we first examined Wnt/□-catenin transcriptional activity using TOP-flash assays. β-catenin transcriptional activity was reduced in untreated ASD compared to control NPCs (**Figure 4a**). Activation of canonical Wnt signaling with 5 mM LiCl, which prevents GSK3-mediated degradation of □-catenin, elevated □-catenin transcriptional activity in ASD and control NPCs. However, □-catenin transcriptional activity was significantly reduced in LiCl-treated ASD NPCs compared to control NPCs (**Figure 4a**), indicating that the cause of reduced □-catenin transcriptional activity is downstream of GSK3. Activation of canonical Wnt signaling with Wnt3A resulted in similar, marked but non-significant elevation of □-catenin transcriptional activity in both control and ASD NPCs (**Figure 4a**), although a similar trend of reduced □-catenin transcriptional activity in the ASD NPCs was noted. These findings indicate that the □-catenin transcriptional activity was reduced in ASD-derived NPCs. We hypothesized that the reduced □-catenin transcriptional activity was responsible for the growth defects displayed by ASD NPCs. To test this hypothesis, we repeated the proliferation experiment in ASD-derived and control NPCs in the presence and absence of LiCl. In the absence of LiCl, all ASD-derived NPC lines displayed faster growth (reduced doubling times) than all control NPC lines. LiCl treatment slowed the growth of ASD-derived NPCs close to doubling times of control NPCs, whereas the growth of control NPCs was unaffected (**Figure 4b**). These findings indicate that the reduced □-catenin transcriptional activity played a functional role in the accelerated proliferation found in ASD-derived NPCs. To test if BRN2 (transcription factor that is downstream of b-catenin activation) levels were similarly affected in ASD NPCs, we performed immunocytochemistry for BRN2 on ASD and control NPCs. The percentage of BRN2^{+} cells was in fact reduced in ASD NPCs compared to controls (**Figure 4c, d**), Western blot analysis confirmed that BRN2 protein levels were reduced in ASD NPCs compared to controls (**Figure 4d-f**). To examine whether exogenous BRN2 rescued the increased rate of proliferation observed in ASD NPCs, we transfected CAG-BRN2 into control and ASD NPCs and performed immunocytochemistry for BRN2 and Ki67. Transfection efficiency was similar between control and ASD NPCs (around 45%). The number of DAPI^{+} cells (as an index of proliferation) in ASD NPCs was similar to controls after BRN2 overexpression (**Figure 4g-j**). The expression pattern of BRN2 and Ki67 in the BRN2 transfected ASD NPCs resembled that of control NPCs, providing additional support for the direct regulation of proliferation of autistic NPCs by BRN2.

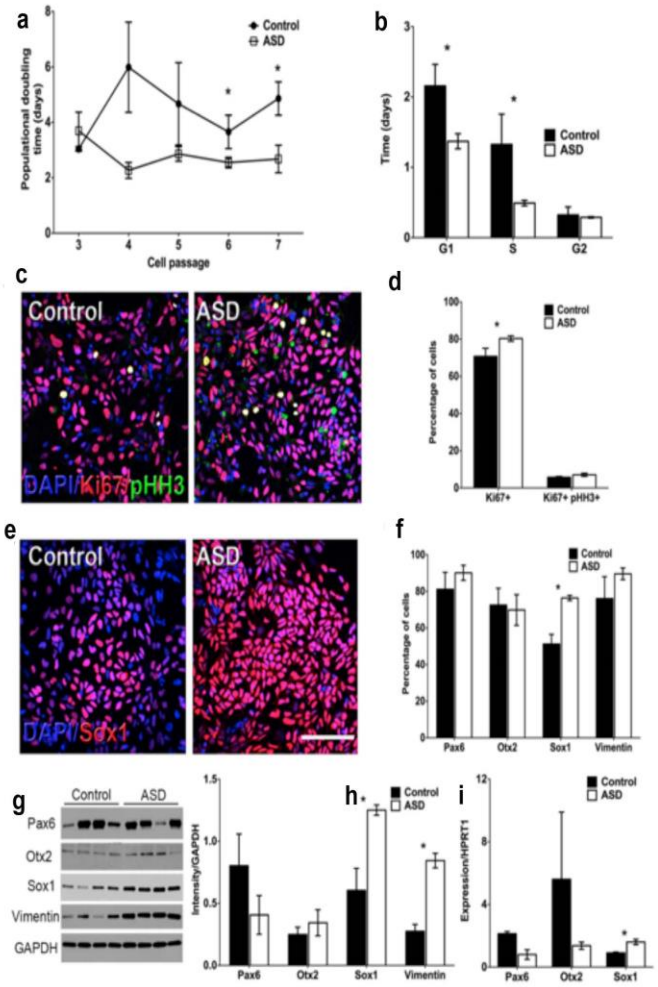

Figure 3: (**a**) iPSCs from ASD and control were differentiated to NPCs. From passages 2 to 6 cells were plated at the same density and population-doubling time at each passage was calculated. Results of 5-6 lines (2 clones per line) are presented as mean±SEM (*p=0.02). (**b**) Adherent monolayer NPCs from control and ASD iPSCs were dissociated, counted for calculation of population doubling time and prepared for cell cycle analysis. Results are presented as the time spent in each cell cycle stage (n≥4, mean±SEM, ANOVA $p<0.04$, post-hoc $p<0.04$ for comparing the time spent in G1 phase in the ASD NPCs with those of the control NPCs, respectively). (**c**) Control and ASD NPCs were immunostained with DAPI (Blue), anti-pHH3 (Green) and anti-ki67 (Red) (Scale bar: 200um), Representative images of the staining are shown. (**d**) Quantification of the percentage of $Ki67^+$ and $Ki67^+pHH3^+$ labeled cells are presented as mean±SEM (n≥5; *$p<0.03$ for comparing the results of the ASD with those of the control NPCs). (**e**) Representative images of the NPC staining for Sox1 (Scale bar: 200□m). (**f**) Quantification of the percentage of $Pax6^+$, $OTX2^+$, $Sox1^+$ and $Vimentin^+$ labeled cells is presented as mean±SEM (n≥5; *$p<0.006$ for comparing the results of the ASD with those of the control NPCs). (**g**) Representative immunoblot of control and ASD-derived NPCs. (**h**) The levels of Pax6, OTX2, Sox1 and Vimentin, which were normalized to GAPDH levels, were quantified and results are presented as mean±SEM (n≥5; *$p<0.007$ for comparing the results of the ASD with those of the control NPCs). (**i**) RNA of control and autistic NPCs was extracted and RT-PCR was performed. The levels of Pax6, OTX2, Sox1, which were normalized to HPRT1, are presented as mean±SEM (n≥3; *$p<0.04$ for comparing the results of the ASD with those of the control NPCs).

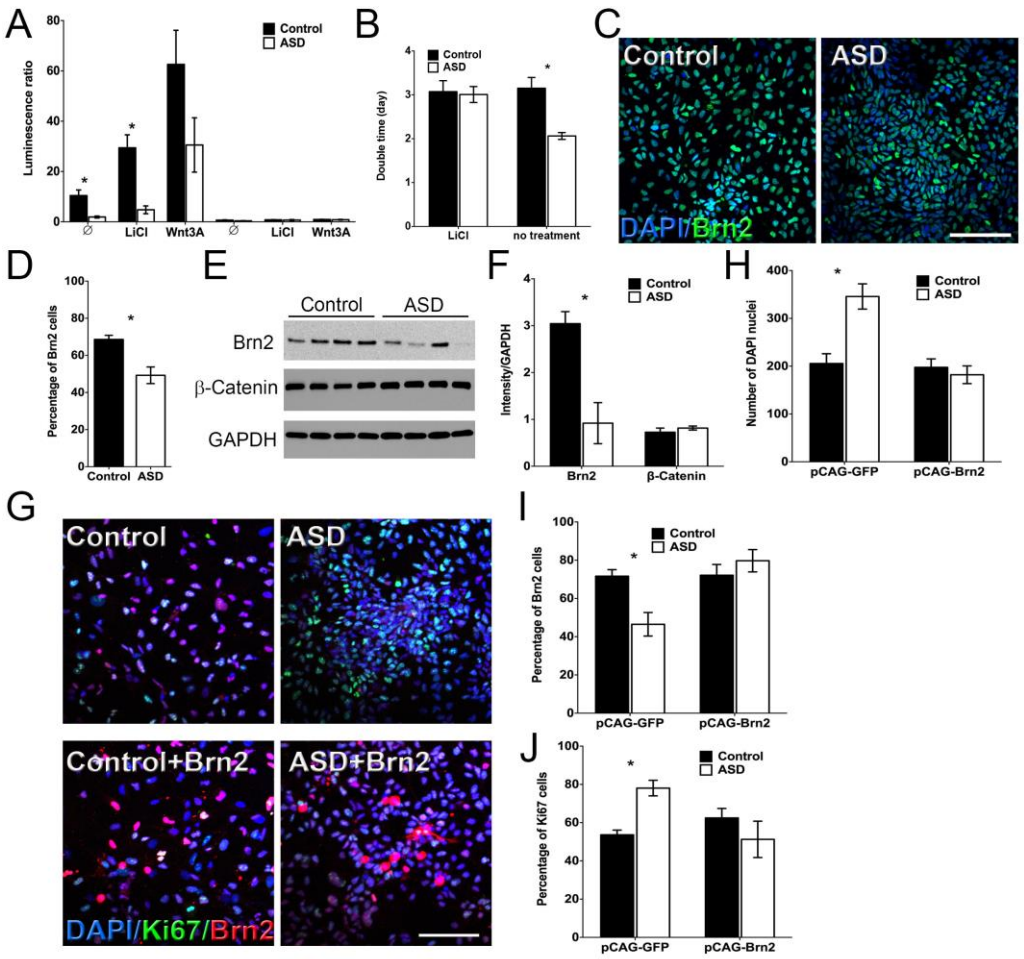

Figure 4. Regulation of NPC proliferation by the Wnt pathway. (**A**) Control and ASD NPCs were transfected with TOP-Flash and firefly renilla reporters and treated with either 5 mM LiCl or 100 ng/ml Wnt3A. Results are presented as mean ± SEM (n≥5, *p<0.04 for comparing the luminescence ratio in the ASD NPCs with those of the control NPCs). (**B**) Doubling time of control and ASD NPCs, treated or not with 5 mM LiCl. Results are presented as mean ± SEM (n≥5, ANOVA<0.05 *p<0.05 for comparing the ASD NPCs doubling time with control NPCs). (**C**) Control and ASD NPCs were fixed and immunostained for Brn2 and representative images of the staining are shown (Scale bar: 200 □m). (**D**) Quantification of the percentage of $Brn2^+$-labeled cells is presented as mean±SEM (n≥5; *p<0.001 for comparing the results of the ASD with those of the control NPCs). (**E**) Representative immunoblot of control and ASD-derived NPCs that were lysed and immunoblot for Brn2, □-catenin and GAPDH. (**F**) The levels of Brn2 and □-catenin, which were normalized to GAPDH levels were quantified and results are presented as mean ± SEM (n≥5; *p<0.03 for comparing the results of the ASD with those of the control NPCs). (**G**) Representative images of pCAG-Brn2 transfected control and ASD-derived NPCs (Scale bar: 200 □m). The number of $DAPI^+$ nuclei (**H**) and the percentage of $Brn2^+$ (**I**) and $ki67^+$ (**J**) cells were measured. Results are presented as mean ± SEM (n≥4, ANOVA<0.02 *p<0.05, comparing the results of the GFP-transfected ASD NPCs with those of the control and the Brn2 transfected autistic NPCs).

The NPC lines from all patients and controls were generated at Dr. Gage laboratory, Salk Institute, La Jolla, CA; all the proliferation tests and β-catenin/BRN2 transcriptional activity tests, immunocytochemistry, western blot and qPCR experiments (**Figures 3 and 4**) described on **Task 1b** were performed in the lab of Dr. Wynshaw-Boris laboratory, UCSF, San Francisco, CA / Case Western Reserve University, Cleveland, OH.

1c. *Perform neuronal differentiation using the iPSC clones characterized in 1a and analyze neuronal maturation using the methods described below (months 8-16).*

We performed differentiation experiments to begin analyzing the neuronal maturation in ASD versus controls. We hypothesized that the proliferation defects observed in ASD NPCs could result in abnormal neuronal differentiation. Therefore, we examined the earliest stages of neuronal differentiation in control and ASD NPCs following 1, 2 and 4 weeks of differentiation. Differentiated NPCs were fixed at the indicated time points and immunocytochemistry was performed for TUJ1 and Doublecortin (DCX) (**Figure 4a**). After 1 week of differentiation, the percentages of TUJ1 and DCX were higher in the ASD samples compared to controls (**Figure 4b, c**). The levels of TUJ1 protein after one week of differentiation were also elevated in ASD compared to control samples by Western blot analysis (**Figure 4d, e**), similar to immunocytochemistry, supporting premature differentiation of ASD NPC. However, differentiation for 2 or more weeks did not reveal differences in the percentage of differentiated cells between ASD and control samples (**Figure 5a-c**).

Evidence from the literature suggests an imbalance in excitatory versus inhibitory signals in developing ASD [5,6]. To examine whether the ASD-NPCs led to a change in excitatory versus inhibitory cell fate, we measured Glutamatergic (NGN2) and GABAergic (MASH1, DLX2, OLIG2 and NKX2.1) progenitor markers in ASD and control NPCs. A reduction in the percentage of $NGN2^+$ NPCs in ASD NPCs compared to controls was observed (**Figure 5f, g**). In contrast, markers of inhibitory precursors present in the subpallium (MASH1, DLX2 and NKX2.1) were up-regulated in ASD compared to control NPCs. However, OLIG2, another subpallium marker, was unchanged between control and ASD NPCs (**Figure 5g**). Together the results described above indicate that ASD neurons start the differentiation program earlier and that could have important implications to proper neuronal maturation and function.

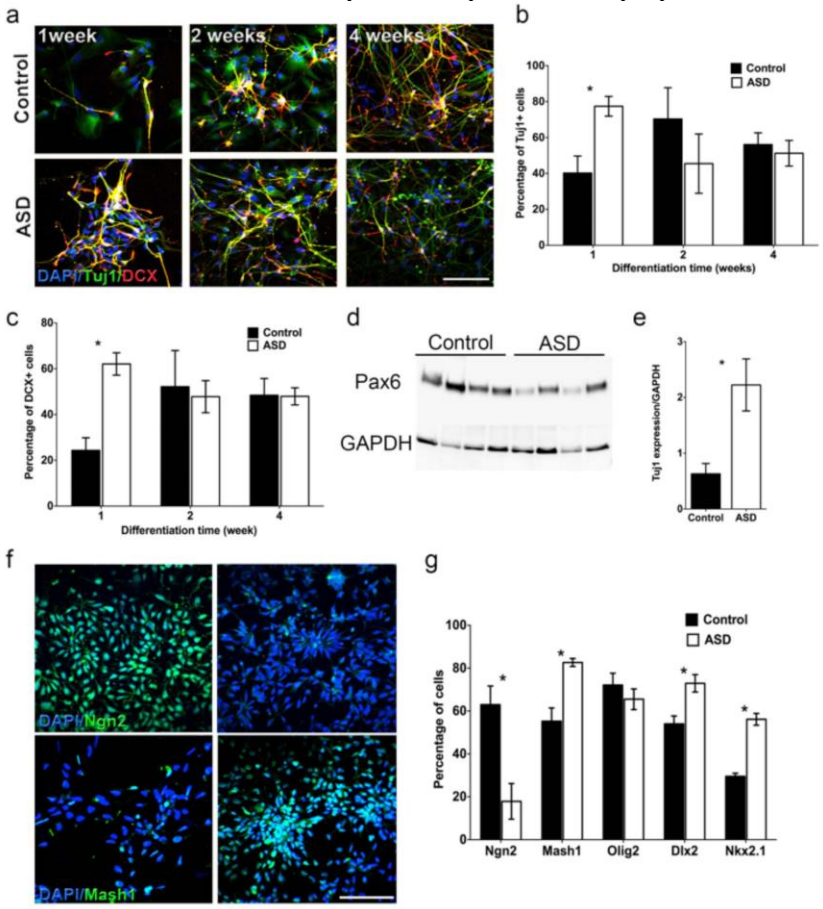

Figure 5. Neuronal differentiation of iPSCs. (**a**) Control and ASD NPCs were differentiated into neurons and fixed after 1, 2 and 4 weeks. (Scale bar: 200 m). The percentages of $Tuj1^+$ (**b**) and DCX^+ (**c**) cells were measured and results are presented as mean±SEM (n=4, AVOVA<0.02 *p<0.04, comparing the results of ASD neuron with those of the control and neurons). (**d**) Control and ASD NPCs were differentiated for 1 week after which cells were lysed and immunoblot for Tuj1 and GAPDH and representative blot is presented. (**e**) The levels of Tuj1, which were normalized to GAPDH levels, were quantified and results are presented as mean±SEM (n=4; *p<0.02 for comparing the results of the ASD with those of the control neurons). (**f**) Representative images of the control and ASD NPCs immunostained for Ngn2 and Mash1. (Scale bar: 200 m). (**g**) Quantification of the percentage of $Ngn2^+$, $Mash1^+$, Olig2, $Dlx2^+$ and $Nkx2.1^+$ labeled cells is presented as mean±SEM (n≥5; *p<0.03 for comparing the results of the ASD with those of the control NPCs).

We then tested the synaptogenesis from mature neurons (6-8 weeks after differentiation). We did not detect a significant alteration in ASD neuronal survival after differentiation when compared to controls, as measured by MAP2 staining. We detected differential expression of excitatory VGLUT1 (vesicular glutamate transpoter-1). Specifically, we found a clear reduction in density and sizes of both Synapsin and VGLUT1 puncta from ASD neurons, suggesting a defect in vesicular glutamate transport in ASD cultures (**Figure 6)**. To confirm the specificity of glutamatergic neurons in our cultures, we demonstrated that VGLUT1 puncta were mostly adjacent to the postsynaptic density-95 (PSD95) protein, a postsynaptic glutamatergic marker (**Figure 6).**

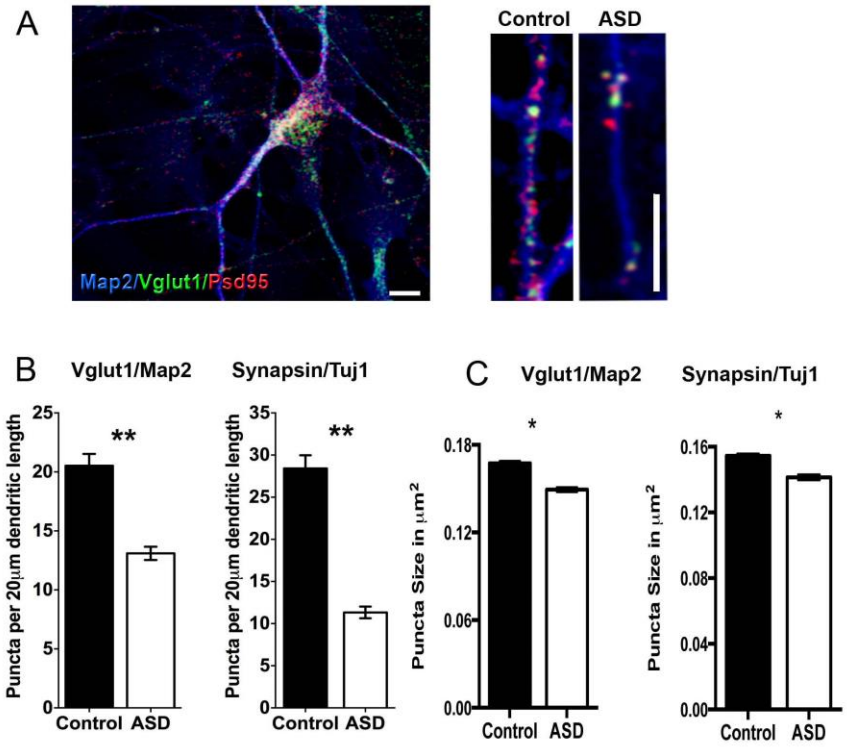

Figure 6. Altered levels of inhibitory and excitatory neurons in ASD neuronal networks. (**A**) Representative images of ASD and control neurons showing Vglut1/Psd95 puncta on Map2 neurites (Scale bar: 5 μm). Bar graphs show decreased synaptic density (**B**) and Puncta size (**C**) in ASD (n=7 individuals, total of 13 lines) compared to control neurons (n=5 individuals, total of 10 lines). *p<0.05 **p<0.01 for comparing the results of the ASD with those of the control neurons.

All the neuronal differentiation assays, immunocytochemistry, western blot and qPCR experiments described on **Task1c Figure 5** were performed in the laboratory of Dr. Wynshaw-Boris laboratory, UCSF, San Francisco, CA / Case Western Reserve University, Cleveland, OH. The experiments of neuronal differentiation and synaptic puncta quantification described on **Task1c**, **Figure 6** were performed and analyzed by the laboratory of Dr. Gage, Salk Institute, La Jolla, CA.

Task 2: Functional characterization of dysregulated pathways uncovered by gene expression from iPSC-derived NPCs and neurons

2a. *Perform single cell qPCR (single cell arrays) to determine the distribution of progenitors and neurons from different brain regions and cortical layers in both ASD and control cells*

Single cell qPCR was not performed because it was not cost effective for a total of 26 lines (8 ASD and 5 controls, 2 clones per individual). Instead, we focused on the functional characterization of ASD and control neurons using a new technology, namely Multielectrode arrays (MEA), that allow for the dynamic detection of neuronal network changes in neuronal cultures from all ASD and neurotypical individuals simultaneously and over time (**Figure 7**). Connectivity defects has been commonly observed in postmortem ASD brains, but connectivity cannot be studied during early stages of embryogenesis. Unlike single-cell patch clamp recordings, multi-electrode arrays (MEA) allow for the dynamic interrogation of how human-derived neurons behave in circuits. We plated control and ASD NPCs to mature in MEA dishes and recorded their activity over time. After 30 days, the total number of spikes in control and ASD neuronal networks was similar. As the cultures matured, the number of spikes increased in control neurons but the numbers of spikes in ASD did not, leading to a significant difference between ASD and control networks (**Figure 7A, B**). After 50 days, we also detected a reduction in the number of synchronized bursts, i.e., spikes that were not singular or random (sequential 10 spikes over 100 ms) in the ASD cultures (**Figure 7C**). While the number of network bursts was variable at 30 days of maturation, with a tendency toward more synchronized events in control neurons, within 50 days of maturation this difference was 6 times higher in control compared to ASD neurons and significant (**Figure 7C**). We then treated the cells with IGF1 (Insulin growth factor 1), a drug that has been previously shown to rescue synaptic deficits in other ASD monogenetic syndromes (Ex. Rett and Phelan-McDermid Syndrome) and is currently in clinical trials for idiopathic ASD [2,7]. The neuronal cultures were treated with IGF1 starting on day 35 of differentiation. Collectively, ASD patients show a tendency to improve neuronal spike number that became significant at day 72 of differentiation (**Figure 7D)**. Interestingly, when we looked at individual patients' response to the drug, while most patients improved the neuronal activity APEX did not show any response (**Figure 8**). Further investigation should clarify the mechanistic reasons for such drug response variation, but nonetheless, the assay may have the sensitivity to pre-screen patients for future clinical trials. These results demonstrate an impairment followed by a partial rescue of network formation in ASD-derived neuronal cultures. The experiments described on **Task 2a, Figure 7 and 8** (Multielectrode Array experiments) were performed by the laboratory of Dr. Gage, Salk Institute, La Jolla, CA.

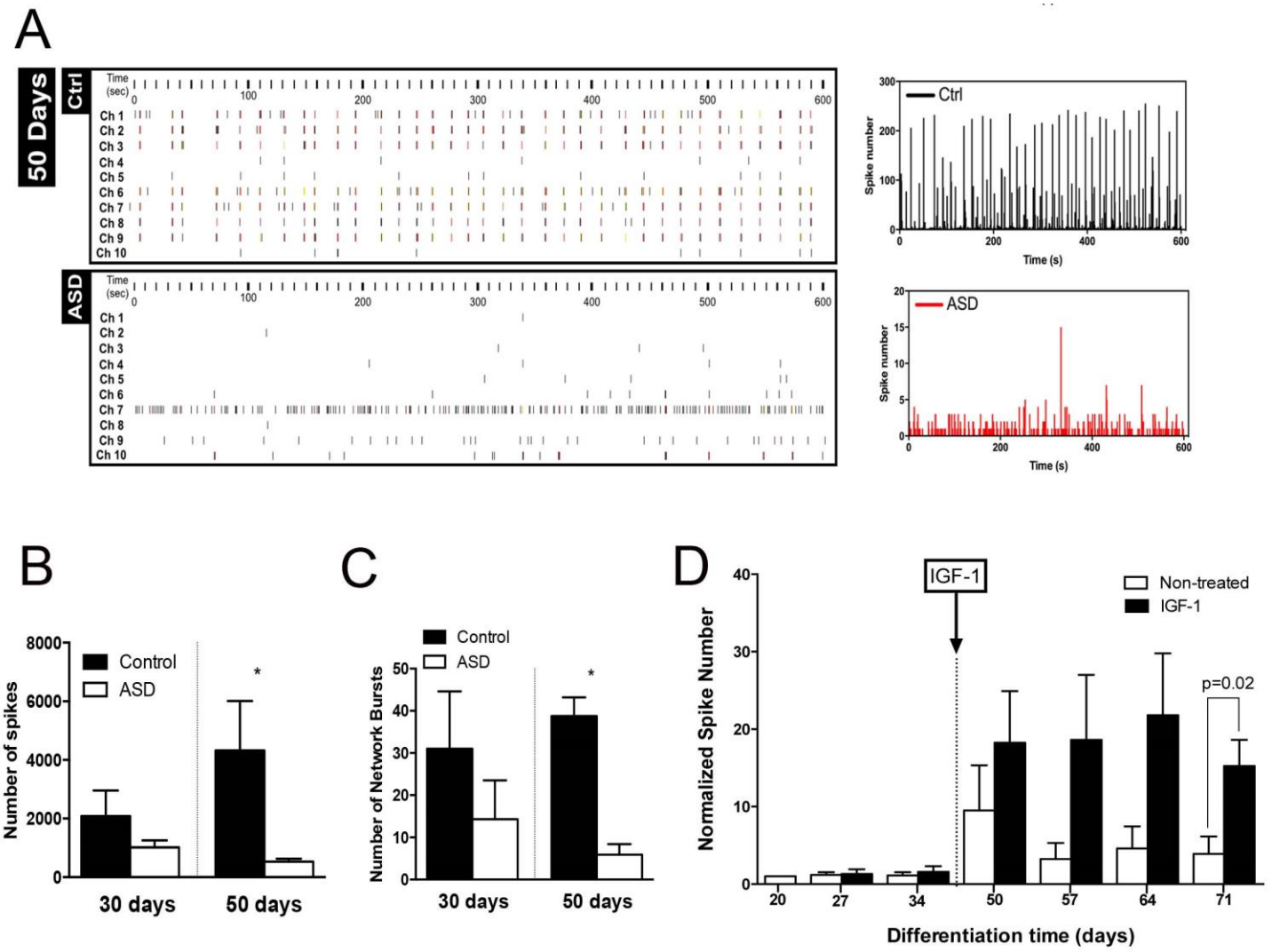

Figure 7. Functional defects in ASD-derived neuronal networks. (**A**) Overlay of a representative XY graph generated from the raw data of a spike raster plot, using the number of spikes recorded over 10 minutes at 50 days of culture maturation. (**B**) Total number of spikes from data obtained from controls (n=6) and ASD (n=10) wells over 30 days and controls (n=4) and ASD (n=9) at 50 days over 10 minutes of recording. Results are presented as mean ± SEM (*p=0.0046 for comparing the results of the ASD with control networks). (**C**) Number of network bursts from wells that were able to generate bursts (10 spikes over 100 ms). Results are presented as mean ± SEM (*p<0.0001 for comparing the results of the ASD with control networks). (**D**) ASD neuronal cultures were treated with IGF1 as indicated in the graph (arrow) and was kept o the cultures for the duration of the experiment.

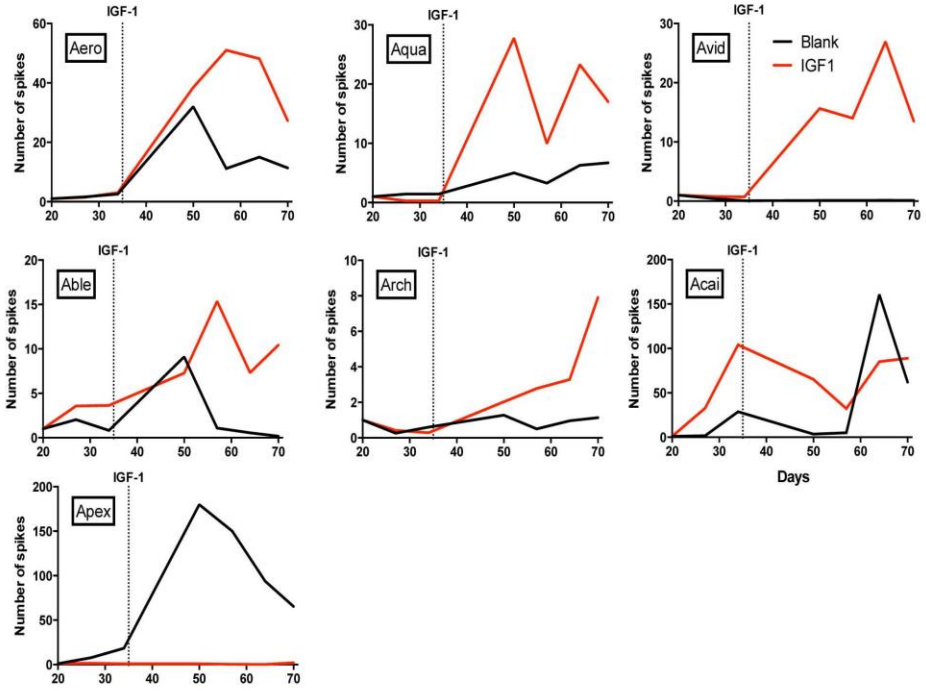

Figure 8. Multielectrode array activity showing Examples of MEA spike activity tracings from each ASD patient with and without IGF1 treatment showing different sensitivities to the drug.

2b. *High throughput sequencing of messenger RNA from differentiated population*

Strong evidence implicates a convergence of pathways at the transcriptome level in postmortem brains from ASD patients [8,9]. Therefore, we performed RNA sequencing analysis in iPSCs and in iPSC-derived NPCs and neurons to evaluate whether any convergent transcriptional alterations could be identified to be associated with early brain overgrowth in ASD during development in this in vitro model. At the transcriptome level, samples were explicitly separated into 3 distinct clusters by cell-type differences based on the top 2 principal components, strongly supporting the reproducibility of our iPSC generation and neural differentiation procedures (**Figure 9 A, B**).

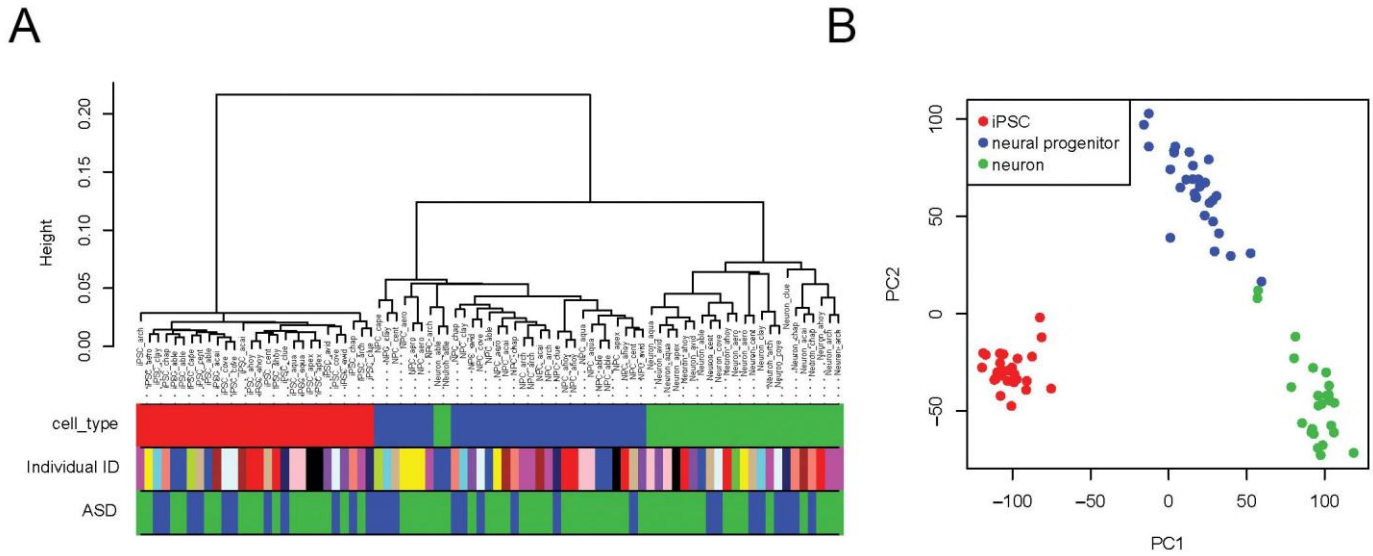

Figure 9: Gene expression analysis in iPSCs and derived cell types. (**A**) Clustering of samples based on inter-sample Spearman correlation using log2 transformed RNA seq read counts. Samples were clustered by cell type differences as shown on the top color bar. Red: iPSCs; blue: iPSC-derived neural progenitors; green: iPSC-derived neurons. Different subjects are indicated using different colors in "Individual ID" color bar. In the "ASD" color bar, green bars represent cell lines derived from patient and blue bars represent cell lines from controls. (**B**) Sample separation based on the top two principal components of genome-wide expression profiles.

We first conducted a standard differential expression (DE) analysis to evaluate individual gene expression pattern changes at the NPC and neuronal stages. We identified 71 genes that were significantly differentially expressed in ASD compared to controls at the NPC stage and 154 genes at the neuronal stage, which by hierarchical clustering clearly distinguished the ASD cell lines from controls (**Figure 10A**). The expression fold changes of the top dysregulated genes are shown in **Figure 10B**.

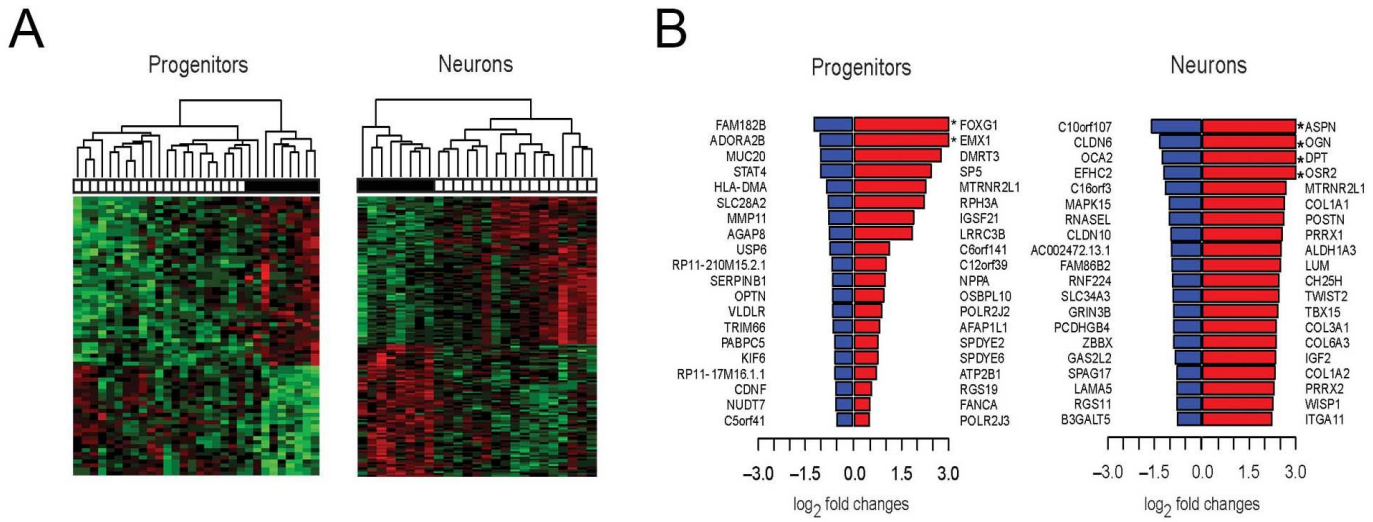

Figure 10: Gene expression changes in neurons and NPCs derived from idiopathic ASD Individuals with macrencephaly. (**A**) Hierarchical clustering using the differentially expressed (DE) genes identified in NPCs (left) and neurons (right). The heatmap shows color-coded scaled expression values, up-regulation in red and down-regulation in green. Each column represents a line from an iPSC clone. The horizontal bar on the top shows disease status: white cell lines are derived from ASD cases, and black represents cell lines from controls. (**B**) Log2 transformed fold changes of the top 20 down-regulated (blue) and top 20 up-regulated (red) genes in patient neural progenitors (left) and neurons (right) as compared to controls. Genes highlighted with * have log2 fold change > 3.

For the experiments described on **Task2b** (**Figures 9 and 10**), all the RNA preparation and isolation was performed in the laboratory of Dr Gage, Salk Institute, La Jolla, CA and the RNA analysis was performed in collaboration with Dr. Geschwind, University of California, Los Angeles, CA.

2c. *Sequencing examination using gene ontogeny pathway analysis*

To reveal the biological pathways associated with the differentially expressed genes, we performed GO enrichment analysis. We found that the up-regulated genes in ASD progenitors were significantly enriched for GO category of brain development, which agrees with the observations of the high NPC proliferation rate and differentiation defects in ASD cultures (**Figure 11A, B**). At the neuronal stage, the up-regulated genes in ASD were enriched for the GO categories related to extracellular matrix, whereas the down-regulated genes were significantly enriched for the GO categories of cilium and axoneme, consistent with the observed synaptic dysregulation (**Figure 11C, D**).

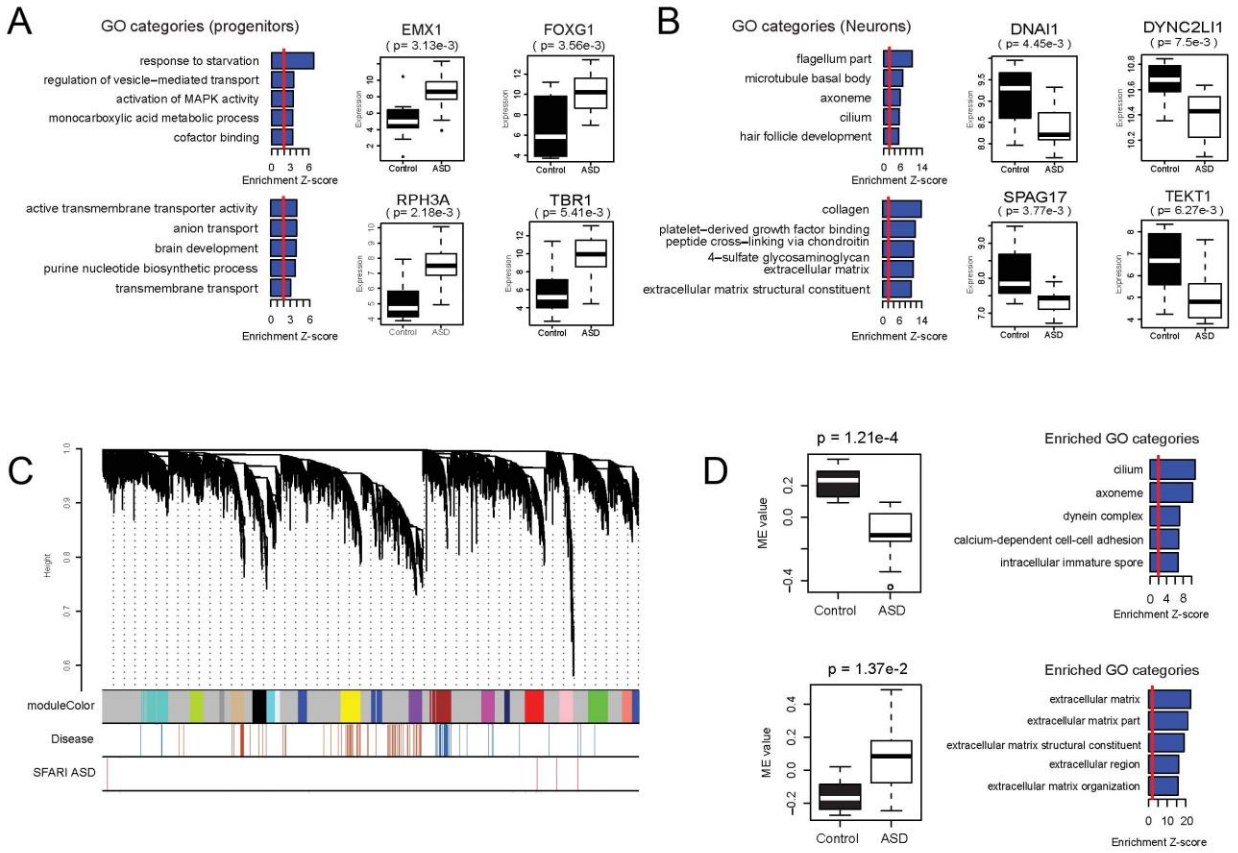

Figure 11: Gene ontology expression analysis in iPSCs and derived cell types (**A**) and (**B**) Barplots showing the enrichment z-scores of the top 5 enriched gene ontology (GO) categories in the down-regulated genes (top) and up-regulated genes (bottom) in ASD samples, respectively. (**C**) Boxplots showing the gene expression patterns of the 4 up-regulated genes in patient progenitors that contribute to the enrichment of the GO category "brain development". (**D**) Expression pattern of the genes involved in the enrichment of GO category "axoneme" among the down-regulated genes in patient iPSC-derived neurons.

To explore the network organization of the transcriptome [10-12], we next applied a Weighted Gene Co-expression Network Analysis (WGCNA) to provide a higher order view of the biological processes altered in the patient cells. Given the substantial transcriptomic alterations in the patient-derived neurons, we mainly focused on determining the gene co-expression organizations at the neuronal stage. We identified 17 gene co-expression modules in the assigned co-expression network (each labeled in a different color). We also observed a striking clustering pattern of the case-associated genes and known ASD susceptibility genes (curated from SFARI database), respectively, upon the identified co-expression structure by plotting the module assignment under the gene clustering dendrogram (**Figure 12A, B**).

Comparing the expression patterns of the modules between ASD and controls, we found 4 modules that were significantly associated with ASD status (FDR <0.1): brown, tan, purple, and magenta (**Table 1**). Remarkably, known autism candidate genes were significantly enriched in these autism-correlated modules. Genes that were commonly affected by ASD-associated CNVs were overrepresented in the brown module (OR=1.5, enrichment p-value=0.02), whereas the tan module was enriched for genes known to be affected by ASD-associated protein-disrupting and missense rare de novo variations (RDNVs) (OR=1.6, p-value=0.02). Because co-expressed genes imply co-regulation, our results provide further evidence for the suggested convergent transcriptional regulation in ASD [9].

Table 1: Modules that were significantly associated with ASD status

Module	ASD association	p-value	FDR	Module Size	direction	Top 3 GO enriched				
Brown	-0.76	1.21E-04	2.18E-03	591	down	cilium	axoneme	dynein complex	calcium−dependent cell−cell adhesion	intracellular immature spore
Tan	0.53	1.37E-02	6.40E-02	360	up	extracellular matrix	extracellular matrix part	extracellular region	extracellular region	extracellular matrix organization
Purple	0.52	1.24E-02	6.40E-02	380	up	RNA processing	mRNA metabolic process	spliceosomal complex	RNA binding	gene expression
Magenta	-0.51	1.42E-02	6.40E-02	382	down	positive regulation of Rap GTPase activity	response to glucose stimulus	negative regulation of insulin secretion	multicellular organismal response to stress	fructose metabolic process

Since ASD NPCs exhibited abnormal differentiation phenotypes, we evaluated whether there were dynamic expression changes in patient cells upon differentiation. Our analysis identified 35 genes showing significant differences in their expression trajectories between ASD NPCs and controls in the progenitor to neuron transition ($p<0.005$) (**Figure 12C**). These genes were significantly enriched for voltage-gated cation channels (**Figure 12D**), including CACNG5, KCNA6, KCNC2, and KCNIP2. As shown in **Figure 12E** and **F**, those channel genes were up-regulated in control cells, but this increase was attenuated in the ASD cells. These data further implicate voltage-gated cation channel dysregulation in ASD neural differentiation, consistent with decreased excitatory glutamatergic synapses, likely affecting synaptic transmission.

For the experiments described on **Task2c** (**Figures 11, 12 and Table 1**), all the RNA preparation and isolation was performed in the laboratory of Dr Gage, Salk Institute, La Jolla, CA and the RNA analysis was performed in collaboration with Dr. Geschwind, University of California, Los Angeles, CA.

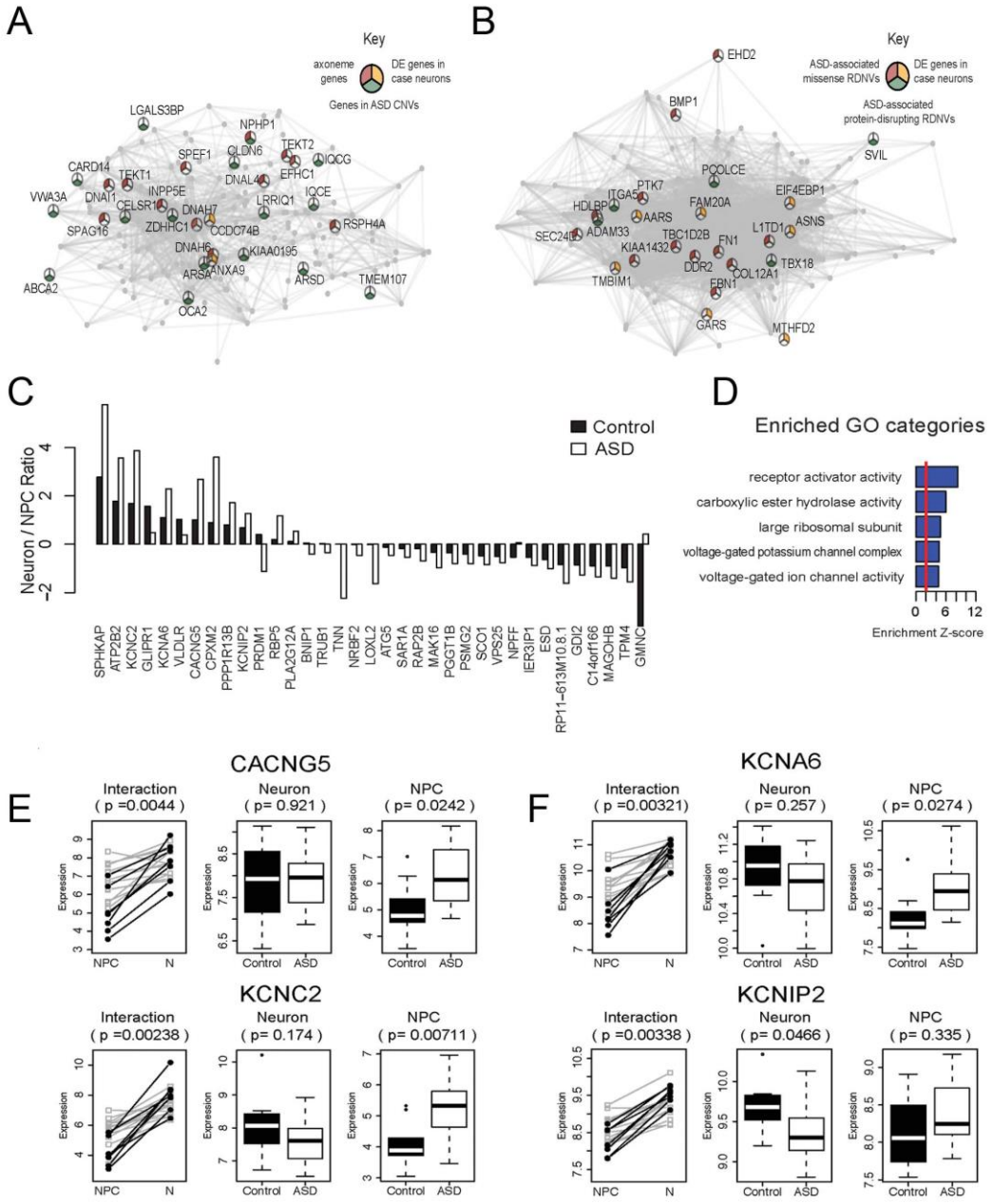

Figure 12: Gene expression and pathways changes in neurons and NPCs derived from idiopathic ASD Individuals with macrencephaly. (**A**) Visualization of the top connections in the brown module, which is down-regulated in ASD neurons. Genes are connected if their pairwise correlation is larger than 0.8. Pie chart: genes in GO category "axoneme" (red); genes in ASD CNVs (yellow); differentially expressed genes ($p<0.005$)(green). (**B**) Visualization of the top connections in the tan module, which shows up-regulation in ASD neurons. Genes are connected if their pairwise correlation is larger than 0.8. Pie chart: genes that are previously identified to be affected by ASD-associated missense (red) and protein disrupting (green) rare de novo variation (RDNVs), and differentially expressed genes ($p<0.005$) (yellow). (**C**) Barplot showing the ratios of neuronal/progenitor expression of the DE genes in the progenitor to neuron transition. Black bars represent the ratios in control samples, and white bars represent the ratios in ASD samples. (**D**) The top 5 enriched GO categories among the genes showing differentiation-dependent expression changes in ASD Individuals vs. controls. (**E** and **F**) Dynamic expression patterns ($\log_2$ transformed read counts) of the genes that show significant differentiation-dependent expression alterations during neuronal differentiation ($p<0.005$) and that are in the GO category "voltage gated ion channel activity." White: cell samples derived from ASD individuals; black: cell samples from controls. P-value in the interaction plot shows the significance of the interaction effect between cell type and disease status. P-values in the neuronal and progenitor plots represent the significance of the difference between ASD cases vs. controls.

4. KEY RESEARCH ACCOMPLISHMENTS:

We are excited to report 5 key important research accomplishments performed during the whole period of the grant, highlighted bellow:

1- We demonstrated that iPSC-derived NPCs from ASD patients with macrencephaly proliferated faster than those derived from controls and that can be explained by a reduction in β-catenin transcriptional activity.

2- We showed that ASD neurons start the differentiation program earlier and that could have important implications to proper neuronal function maturation.
3- We demonstrated that ASD neurons have lower densities of dendritic glutamatergic puncta compared to neurotypical controls, indicating a defect in glutamatergic synapses.
4- We detected a significant deficiency in network connectivity in ASD using the multielectrode array platform (decreased number of neuronal spikes and bursts) that was ameliorated with the addition of IGF1, a drug that is currently in clinical trials for ASD.
5-Using high throughput RNA sequencing analysis we showed that at the progenitor stage, ASD cultures show up-regulation of genes related to brain development, such as EMX1, FOXG1 and TBR1. At the neuronal stage, the genes displaying abnormal expression patterns in ASD were mainly related to voltage-gated cation channel activity, including genes previously implicated in ASD and other mental disorders, such as CACNG5, KCNA1 and KCNA6.

5. CONCLUSION:

The use of iPSCs to study genetic disorders is a powerful tool to dissect molecular and cellular pathways implicated in disease pathology during early stages of human neurodevelopment. However, modeling highly complex idiopathic disorders such as ASD is challenging due to a high level of heterogeneity in the patient population. Here, we took advantage of iPSCs derived from a carefully characterized clinical cohort of ASD patients who have an anatomical phenotypic trait that occurs in about 20-30% of idiopathic ASD: an early developmental enlargement of brain volume, including macrencephaly that is frequently associated with poor prognosis. We reasoned that ASD patients sharing a common phenotype, early developmental brain enlargement ranging from mild to extreme macrencephaly, might share underlying molecular and cellular pathway dysregulation. Our findings described here show that neural progenitor cells (NPCs) derived from ASD-iPSC proliferated faster than those derived from controls and showed reduction in β-catenin transcriptional activity. Additionally, we showed that ASD-derived neurons formed fewer excitatory synapses and matured into defective neuronal networks with less bursting. Importantly, ASD patients showed improved network strength after treatment with IGF1 (a drug that is currently in clinical trial for ASD), but the levels of improvement were unique to the patients, revealing a potential novel assay to pre-screen patients for future clinical trials. Moreover, unbiased gene expression analyses in both NPCs and neurons derived from ASD iPSCs revealed differential gene regulation and molecular pathways, such as voltage-gated calcium channels, related to brain development and disease. Together, our results suggest that, when stratified into measurable endophenotypes, idiopathic ASD can be modeled using iPSC technology to reveal novel cellular and molecular mechanisms underlying brain abnormalities.

6. PUBLICATIONS, ABSTRACTS, AND PRESENTATIONS:

MANUSCRIPT SUBMITTED FOR PUBLICATION

Brennand, Kristen J., M. Carol Marchetto, Nissim Benvenisty, Oliver Brustle, Allison Ebert, Juan Carlos Izpisua Belmonte, Ajamete Kaykas, Madeline A. Lancaster, Frederick J. Livesey, Michael J. McConnell, Ronald D. McKay, Eric M. Morrow, Alysson R. Muotri, David M. Panchision, Lee L. Rubin, Akira Sawa, Frank Soldner, Hongjun Song, Lorenz Studer, Sally Temple, Flora M. Vaccarino, Jun Wu, Pierre Vanderhaeghen, Fred H. Gage, and Rudolf, Jaenish. Creating Patient-Specific Neural Cells for the In Vitro Study of Brain Disorders. *Stem Cell Report*, (2015, accepted)

Xin Tang, Julie Kim, Li Zhou, Eric Wengert, Lei Zhang, Zheng Wu, Cassiano Carromeu, Alysson R Muotri, Maria CN Marchetto, Fred H. Gage and Gong Chen. KCC2 rescues functional deficits of human neurons derived from Rett syndrome patients. *PNAS* (submitted).

Marchetto, M.C., Belinson, H., Tian, Y., Beltrao-Braga, P., Trujillo, C., Mendes, A., Nunez, Y., Gosh, H., Brennand, K., Pierce, K., Pramparo, T., Eyler, L., Barnes, C.C., Courchesne, E., Gage, F.H., Geschwind, D., Wynshaw-Boris, A.* and Muotri, A.R.* Evidence for proliferation and synaptogenesis impairments in neural cells derived from idiopathic autistic patients. * co-corresponding authors

7. INVENTIONS, PATENTS AND LICENSES: Nothing to report

8. REPORTABLE OUTCOMES: Nothing to report

9. OTHER ACHIEVEMENTS:

This award contributed to the production of neurotypical controls and ASD iPS cell lines from 13 individuals listed bellow (and 2 clones each, except for CLUE).
1-AQUA, 2-AHOY, 3-ACAI, 4-AVID, 5-ABLE, 6-AERO, 7-ARCH, 8-APEX (ASD)

10. **REFERENCES:**

1 Takahashi, K. *et al.* Induction of pluripotent stem cells from adult human fibroblasts by defined factors. *Cell* **131**, 861-872 (2007).
2 Marchetto, M. C. *et al.* A model for neural development and treatment of Rett syndrome using human induced pluripotent stem cells. *Cell* **143**, 527-539, doi:10.1016/j.cell.2010.10.016 (2010).
3 Elkouris, M. *et al.* Sox1 maintains the undifferentiated state of cortical neural progenitor cells via the suppression of Prox1-mediated cell cycle exit and neurogenesis. *Stem Cells* **29**, 89-98, doi:10.1002/stem.554 (2011).
4 Alonso, G. Proliferation of progenitor cells in the adult rat brain correlates with the presence of vimentin-expressing astrocytes. *Glia* **34**, 253-266 (2001).
5 Rubenstein, J. L. Three hypotheses for developmental defects that may underlie some forms of autism spectrum disorder. *Curr Opin Neurol* **23**, 118-123, doi:10.1097/WCO.0b013e328336eb13 (2010).
6 Zikopoulos, B. & Barbas, H. Altered neural connectivity in excitatory and inhibitory cortical circuits in autism. *Frontiers in human neuroscience* **7**, 609, doi:10.3389/fnhum.2013.00609 (2013).
7 Shcheglovitov, A. *et al.* SHANK3 and IGF1 restore synaptic deficits in neurons from 22q13 deletion syndrome patients. *Nature* **503**, 267-271, doi:10.1038/nature12618 (2013).
8 Voineagu, I. Gene expression studies in autism: moving from the genome to the transcriptome and beyond. *Neurobiology of disease* **45**, 69-75, doi:10.1016/j.nbd.2011.07.017 (2012).
9 Parikshak, N. N. *et al.* Integrative functional genomic analyses implicate specific molecular pathways and circuits in autism. *Cell* **155**, 1008-1021, doi:10.1016/j.cell.2013.10.031 (2013).
10 Oldham, M. C. *et al.* Functional organization of the transcriptome in human brain. *Nature neuroscience* **11**, 1271-1282, doi:10.1038/nn.2207 (2008).
11 Voineagu, I. *et al.* Transcriptomic analysis of autistic brain reveals convergent molecular pathology. *Nature* **474**, 380-384, doi:10.1038/nature10110 (2011).
12 Konopka, G. *et al.* Human-specific transcriptional regulation of CNS development genes by FOXP2. *Nature* **462**, 213-217, doi:10.1038/nature08549 (2009).

11. **APPENDICES:** Nothing to report